



OPEN

Giant photoluminescence emission in crystalline faceted Si grains

Giuseppe Faraci¹, Agata R. Pennisi¹, Alessandra Alberti², Rosa Ruggeri² & Giovanni Mannino²¹Dipartimento di Fisica e Astronomia, Università di Catania, Via Santa Sofia 64, 95123 Catania, Italy, ²Istituto per la Microelettronica ed i Microsistemi – Consiglio Nazionale delle Ricerche (CNR-IMM), VIII Strada n°5 Zona Industriale, 95121 Catania, Italy.

Empowering an indirect band-gap material like Si with optical functionalities, firstly light emission, represents a huge advancement constantly pursued in the realization of any integrated photonic device. We report the demonstration of giant photoluminescence (PL) emission by a newly synthesized material consisting of crystalline faceted Si grains (fg-Si), a hundred nanometer in size, assembled in a porous and columnar configuration, without any post processing. A laser beam with wavelength 632.8 nm locally produce such a high temperature, determined on layers of a given thickness by Raman spectra, to induce giant PL radiation emission. The optical gain reaches the highest value ever, 0.14 cm/W, representing an increase of 3 orders of magnitude with respect to comparable data recently obtained in nanocrystals. Giant emission has been obtained from fg-Si deposited either on glass or on flexible, low cost, polymeric substrate opening the possibility to fabricate new devices.

Although bulk-Si is an inefficient light emitter, Si nanocrystals have been engineered to luminesce only if of few nanometer in size^{1–3}. The challenge for combining optical and electronic functions in a silicon device, i.e., the implementation of the wide communication bandwidth of photonics with the high electric performance of silicon, remains a topic at the frontier of physics also in this century^{4–6}. The search of stimulated emission of radiation and/or of amplified enhancement in optical systems based on silicon nanocrystals represents one of the most promising field for obtaining photoluminescence amplification in the visible range^{7,8}. In bulk silicon indirect radiative interband transitions are prohibited by the momentum conservation law and require phonon absorption or emission. A possible route for overcoming this difficulty consists of the modification of the electron dispersion equations $E(k)$ for valence and conduction bands, by a precise size confinement of silicon nanocrystals¹. In such cases, the quantum confinement, relaxing the electron momentum, could in principle allow radiation emission not phonon-assisted. In fact, the gap widening of a Si nanocrystal (nc-Si) offers the opportunity of light emission in the visible rather than in the infrared range of the bulk silicon. However, a stimulated PL emission in nc-Si, although observed in several cases, has still a very low efficiency⁹. It should be noted also that it is impossible to obtain a nc-Si monodisperse ensemble, usually spreading over a large range of sizes. Furthermore, nc-Si synthesis occurs after deposition at high temperature well above that compatible with any low cost substrate such as glass or polymeric substrates⁷.

Actually, recent activities have focused on light generation and amplification, using Raman effect in nanostructures, surface enhanced Raman scattering, stimulated Raman amplification in silicon waveguides and realization of a Silicon Raman laser^{10–14}. Previous observations of ultraviolet and visible radiation emission from Si were reported from the contacts of a scanning tunneling microscope. This luminescence relies on the presence of hot electrons in silicon on phononless emission from bulk in the range 2–5 eV¹⁵. In nanostructured Si, photoluminescence spectrum of silicon nanocrystals were reported with increasing intensity and shift to longer wavelengths with smaller nanocrystal sizes. This effect was attributed to a radiative recombination of non-equilibrium electron–hole pairs in a process that does not involve phonons¹⁶. Doping of nc-Si with P and/or B is also a promising alternative^{4,17}. At the same time innovative concepts of photovoltaic solar cells, which in principle could overpass the Shockley-Queisser limit, are based on carrier multiplication or on the capability to extract carriers having an energy greater than the Si band gap before the generated carriers lose their energy reaching the valley of the respective bands and recombine, provided specific nanocrystals are incorporated^{18–21}.

We explore a different approach for obtaining a Si based innovative material, able to emit an intense PL signal in the visible range. Our efforts are dedicated to the realization of a material where photoluminescence is induced and amplified by fostering indirect phonon-assisted transitions over the entire Brillouin zone, via an enormous local temperature increase^{22,23}. With this purpose we synthesise and optimize a material which has two main

SUBJECT AREAS:
SILICON PHOTONICS
APPLIED PHYSICS
NANOPARTICLES
ELECTRONIC PROPERTIES AND
MATERIALSReceived
15 May 2013Accepted
24 July 2013Published
23 September 2013Correspondence and
requests for materials
should be addressed to
G.F. (giuseppe.
faraci@ct.infn.it) or
G.M. (giovanni.
mannino@imm.cnr.it)



characteristics i) be formed by nanoparticles with a specific shape having a high volume to surface ratio so to obtain a controlled and high local temperature ii) be composed of almost isolated nanoparticles, not strictly in contact to other nanoparticles or with a surrounding external matrix, in order to hamper thermal exchange.

Results

The material is prepared by exploiting the capabilities of a low pressure and high density plasma (see Fig. 1a–b)^{24,25}. We use an inductively coupled plasma reactor to synthesise large, defect free, crystalline Si particles few hundred nanometers each with a unique octahedral shape and minimal dispersion in size with a Full Width Half Maximum (FWHM) < 5%. It has to be noted that this size is much larger than any previous data in the literature whereas the shape is still consistent with theoretical studies^{26–28}. Thanks to an accurate and reproducible process, we have assembled them in a layer we call faceted-granular Si (fg-Si). This material is formed by faceted micrograins in a way that each particle is not fully in contact with the surrounding ones but rather form agglomerates or columns, in a diluted/porous configuration. The layer thickness might be varied on purpose from a sub-monolayer of nanoparticles up to a micrometer-thick layer (a typical fg-Si layer structure is shown by transmission electron microscopy images in Fig. 1c on top). By using

X-ray diffraction analysis (fig. 1c bottom) we found that the fg-Si layer is built by particles preferentially landed with the largest (111) face of the octahedron parallel to the substrate stacked in columns. The layer is composed of octahedra of a single size having the edge of 110 nm with empty spaces in between. During the deposition process, it is noteworthy that the substrate is maintained at only 50°C (see methods for details) and this allowed us to perform deposition and successive PL measurements either on glass or on polymeric substrate, Polyethylene naphthalate (PEN) in this experiment.

Fig. 2 shows the enormous PL spontaneous emission stimulated by a He-Ne laser beam at 632.8 nm wavelength. The yield depends mainly on the layer thickness which is controlled by the plasma process time, since the overall height of the layer, in terms of stacked grains, determines the local temperature increase. We have indeed demonstrated that a fg-Si layer gives at room temperature an enormous PL emission several order of magnitude larger than the bulk silicon, where no PL is detected at all. Furthermore it is as well noteworthy that the substrate is not intentionally heated nor any substrate heating occurs, thus we were able to reproduce the same PL luminescence increase on low melting point polymeric substrates and on glass.

The main peak visible in the PL spectrum corresponds to the Raman Stokes peak at $E_S = E_0 - E_p = 1.9$ eV (i.e. 654 nm). The

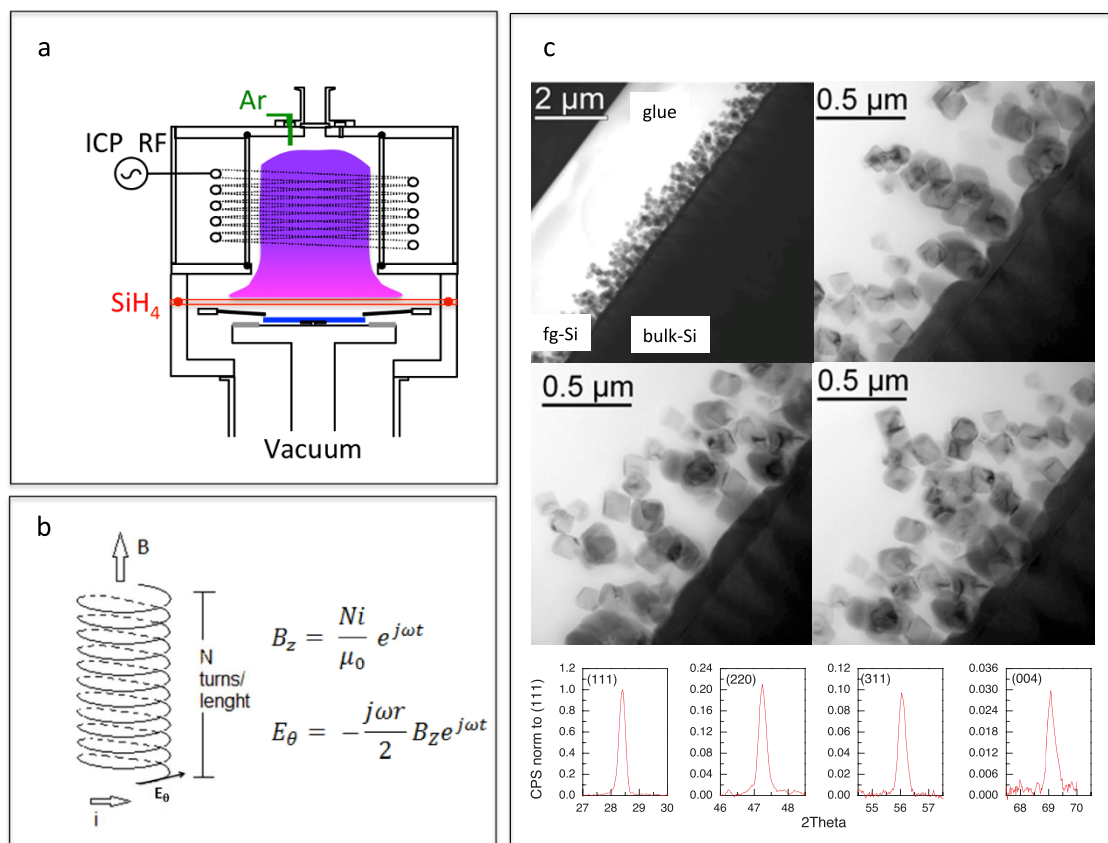


Figure 1 | (a), schematic view of the inductively coupled plasma chemical vapour deposition system with its typical vertical geometry. (b), the RF applied to a solenoid produces a magnetic field perpendicular to the sample and induces a tangential electric field. This scheme, contrary to parallel plate configuration, ensures the plasma is highly ionised and capable to form large crystalline nanoparticles competitively to Si amorphous deposition; (c), electron transmission (top) and x-ray diffractogram (bottom) of a typical fg-Si layer deposited in 1 hr of processing. Each TEM image shows (from bottom to top) the Si bulk substrate, a thin amorphous Si layer and the fg-Si layer formed by agglomerates and columns of Si nanoparticles (octahedra) in diluted concentration and mainly surrounded by empty spaces. On top of the fg-Si layer there is the glue residual after thinning of the TEM specimen. The major axis length of the octahedron is of ≈ 200 nm, the edge of each face is ≈ 110 nm. Individual grains appear to be different from each other but this is indeed due to the random cut of each octahedron along the specific plane during sample preparation. At the bottom of the fg-Si layer is visible a thin amorphous Si layer. Layer thickness and particle concentration is varied according to process parameters. From x-ray diffractogram, the planar distance deduced by the Bragg law is only slightly relaxed by 0.2% with respect to that of bulk Si. Peak area ratios to (111) direction with respect to a random polycrystalline layer attests a preferential landing of particles with the largest (111) face of the octahedron parallel to the substrate.

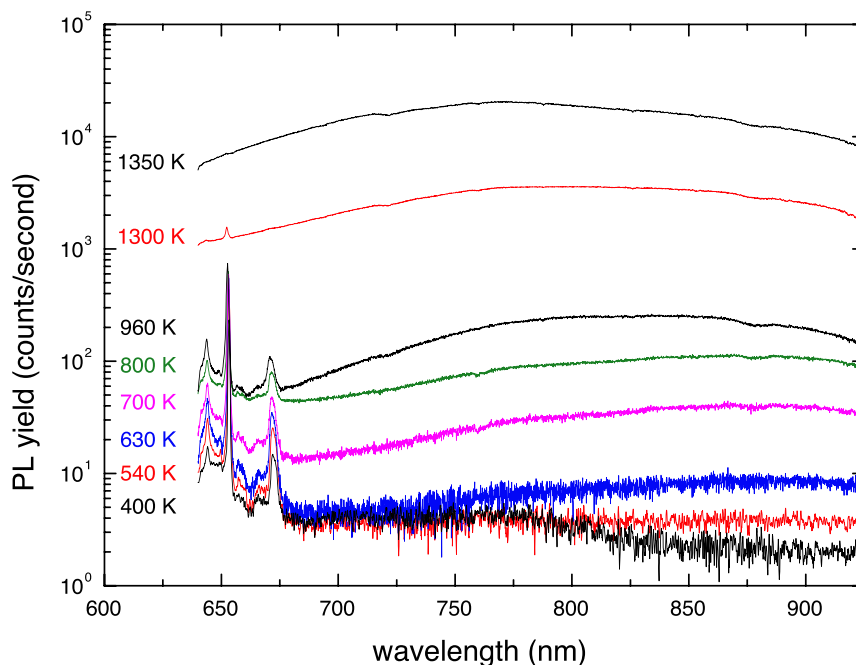


Figure 2 | (a), Photoluminescence emission spectra from fg-Si layer. The PL yield dramatically increases as a function of the temperature, with a broad peak centred at about 770 nm. Afterwards a rapid decrease is observed with a minimum around 940 nm. Being the laser energy at $E_0 = 1.963$ eV (633 nm) and the TO phonon energy $E_p = 63$ meV the main peak visible in the PL spectrum corresponds to the Raman Stokes peak at $E_S = E_0 - E_p = 1.9$ eV (i.e. 654 nm). The spectrum clearly shows the satellite peaks around 645 nm and 670 nm produced by overtones of two acoustical or optical phonons respectively²⁹. Note also the quenching of the Raman peak at high temperature, because of the augmented number of phonons absorbed by indirect electron excitations.

spectrum clearly shows the satellite peaks around 645 nm and 670 nm produced by overtones of two acoustical or optical phonons respectively²⁹.

The Raman peak position and linewidth for our typical sample deposited on glass and on polymeric substrate is shown in Fig. 3a. Both Stokes and anti-Stokes features are displayed in order to check the local temperature under the laser beam. For comparison a Si wafer is also investigated as reported in the same figure. The inset of Fig. 3a demonstrates that the same peak shift and broadening (only the Stokes peak is shown) is obtained in fg-Si deposited on polymeric and glass substrates. We observe a large Raman shift (up to 30 cm^{-1}) with respect to the bulk and a correspondent significant line broadening. If we reduce the laser beam intensity we detect a progressive reduction of the shift and linewidth approaching the bulk values. The local temperature is thus deduced by the ratio between Stokes/anti-Stokes peak area, taking into account the Raman cross section²⁹:

$$\frac{Y_S}{Y_{as}} = \frac{(\omega_0 - \omega_p)^4}{(\omega_0 + \omega_p)^4} \exp\left[\frac{\hbar\omega_p}{kT}\right] \quad (1)$$

where Y indicates the yield, ω_0 the laser frequency, ω_p the phonon frequency, k the Boltzmann constant and T the temperature. From that relationship, the local temperature is calculated as plotted in Fig. 3b as a function of the Raman shift, for a number of different samples and/or irradiation intensities.

The linewidth (FWHM) and high Raman shift (see Fig. 3a) are associated to an increase of the temperature within that part of the layer heated by the laser. In contrast, the bulk Si wafer does not show any variation in temperature, remaining at 300 K at any laser intensity used. No temperature modification is detected whenever the fg-Si is fully embedded in a matrix, as for example an amorphous Si or silicon oxide layer deposited after the fg-Si deposition. The matrix simply acts as a thermal conductor thus preventing any local heating. A similar explanation can be invoked for bulk Si. It is important to remind that the specific layer thickness univocally determines the

temperature locally reached under the laser beam with a variation limited to ± 20 K. Moreover, the size of the individual Si grains composing the layer (few hundred nanometers) is by far larger than that allowing any PL due to size confinement effects^{1,22,23,30,31}.

The fg-Si layer is typically formed by a few crystallites per square micrometer, from 1 to 30 depending on process time used. Calling W_1 the laser power density, I the amplified PL emission as a function of the equivalent layer thickness t_e we write:

$$I = I_0 \exp(gt_e W_1) \quad (2)$$

where g is the amplification factor, I_0 the PL reference emission when $g = 0$, and t_e the fg-Si thickness crossed by the beam. We stress that bulk-Si does not exhibit any temperature increase and no PL, and therefore we use as a reference an fg-Si layer having a PL yield corresponding to $T = 400$ K. With the previous formula, in fact, using the spectra shown in Fig. 2, where PL results up to several order of magnitude larger than the reference sample, we calculate an amplification factor g reaching a value up to 0.14 cm^2/W assuming the following data: $I/I_0 = 5 \times 10^3$, $W_1 = 6$ $\text{mW}/1$ μm^2 , $t_e = 1.0$ μm at the maximum PL yield. Our value is much larger than a similar result (438 cm^2/MW) obtained in the IR range on stimulated Raman scattering in silicon nanocrystals embedded in a silica matrix under non-resonant excitation at infrared wavelengths². Note also that the maximum PL yield is obtained for a sample with an effective layer thickness of 1.0 μm (see Fig. 1).

Discussion

Now we discuss the origin and the relevance of the huge PL increase (see Fig. 4). The local high temperature, caused by the laser beam, is responsible of an enormous phonon production. The temperature increase is enhanced in this innovative material, the fg-Si, by its capability to absorb the radiation being the Si grains quite large but at the same time not closely packed or connected to dissipate the heat produced by radiation absorption itself.

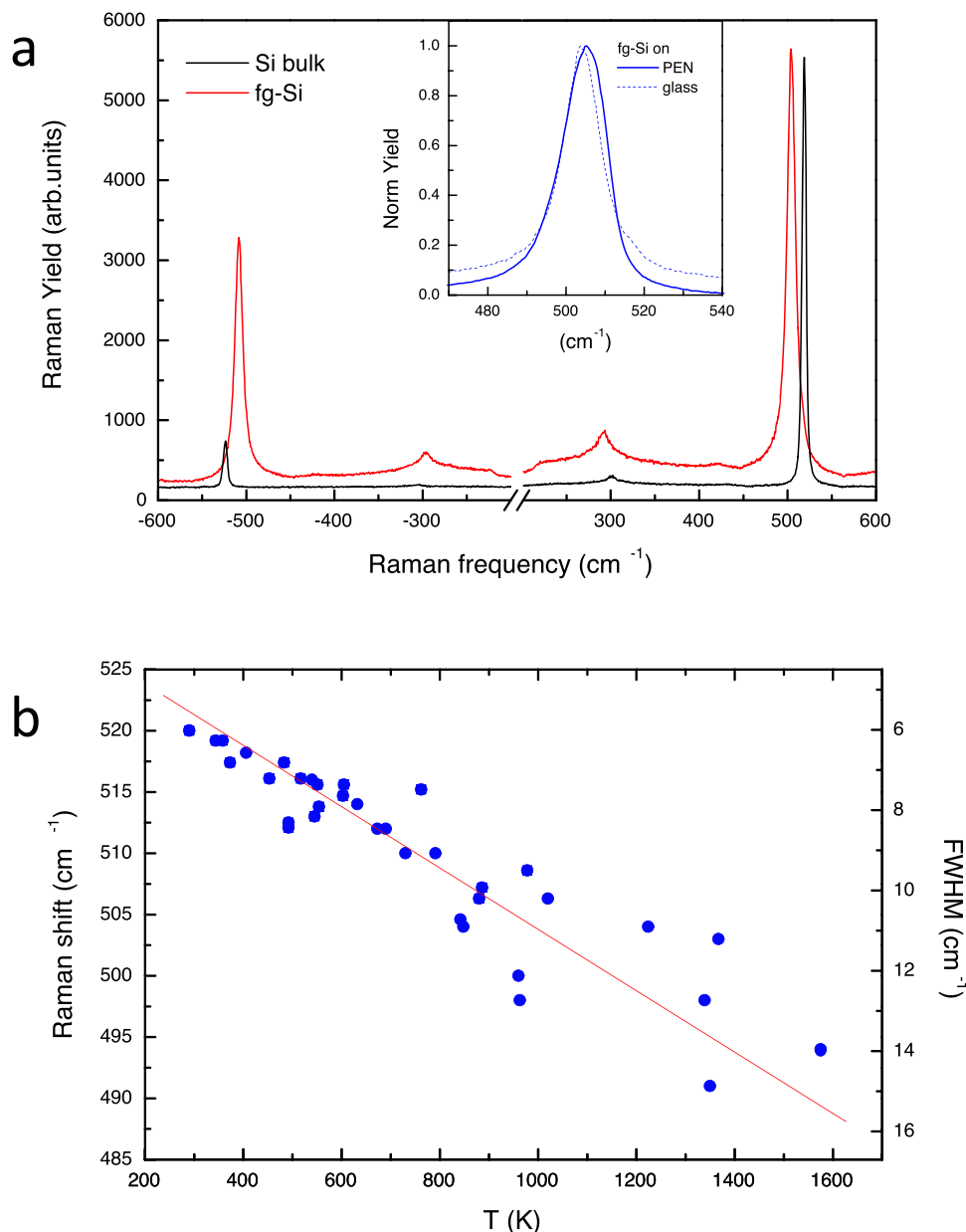


Figure 3 | (a), Typical Raman spectra obtained in bulk-Si and fg-Si layer. Clearly visible the relative shift and broadening corresponding to a temperature calculated according to eq. 1 of 1000 K. The modification of the relative yield provides the local temperature measurement. In the inset we report the Stokes Raman peak spectra measured in fg-Si deposited on glass and polymeric, Polyethylene naphthalate (PEN), substrates. We note that the two peaks have similar position and width. (b), Plot of the Raman shift (left scale) and broadening (FWHM, right scale) as a function of the local temperature. The line is added to guide the eye.

We argue that the thermal conductivity of our fg-Si is very low with respect to the bulk Si. In fact, the breaking of long range order, i.e., the phonon scattering at the surface of the octahedra traps the phonons with consequent increase of local temperature. A detailed investigation of the thermal conductivity as a function of fg-Si layer thickness will be reported elsewhere. However, the local temperature of the micrograins is assumed as a clear indication of the poor thermal conductivity, related to the porosity of the layer.

The phonon population trigger indirect electron transitions over the entire Brillouin zone as permitted by the electron energy increment due to the laser photon absorption and, as a consequence, many electronic excited states appear in silicon conduction band. These in turn decay either directly and/or indirectly with a broad PL emission. Of course, this effect is not allowed at room temperature because of

the limited number of phonons and of the specific form of the electron energy dispersion relations.

Absorption and emission of phonons play a crucial role in the interpretation of the observed effect. In fact, as well known, being the Si an indirect gap semiconductor, it does not present any photoluminescence, at room temperature, because of the limited number of phonons which can stimulate absorption of radiation and consequent PL decay. The ratio of the bosonic population of phonons goes as $n + 1/n = \exp(\hbar \omega_p/k T)$, which at room temperature gives, e.g., a value of 12.4, for the TO energy of 63 meV, whereas at 1350 K the ratio goes down to 1.75. This implies a high emission and absorption at high temperature, but not at 300 K, since the reduced probability of absorption. This in turn prevents PL emission.

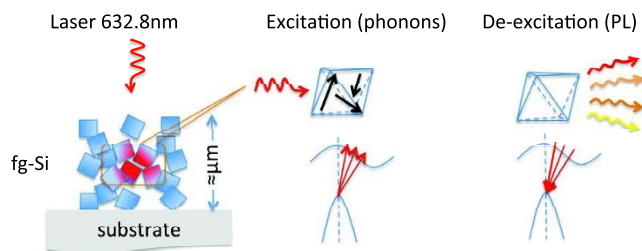


Figure 4 | Schematic view of the PL emission process: (left) the laser radiation heats the micrograins in the fg-Si layer, (center) the scattered photons produce phonons increasing the local temperature. Electron indirect transitions are stimulated, with high number of excitons (e-h couples). (right) Hot carriers decay either directly and indirectly with huge PL emission.

Note also that at high temperature the electron energy dispersion curves are thermally smeared and therefore these absorption and emission processes are easily stimulated.

A further interesting investigation involves the modification of the band for increasing temperature. It is quite obvious that a thermal fluctuation of the order of KT can be considered as an additional modification of the energy band curves. This smearing at 1350 K reaches 0.11 eV a value of the order of 10% of the Si gap. Therefore, for increasing temperature, the thermal energy contributes in favor both of the absorption and emission. In addition, note that the thermal energy influences also the phonon dispersion relations³¹.

A question arises about the contribution of scattered radiation and how it can be distinguished from the PL emission. We point out that the decrease of Raman yield for increasing temperature demonstrates the lowering of scattering cross section of photons by phonons, in favor of indirect electron absorption, with consequent PL increase.

Another observation concerns the degree of thermal exchange and therefore the maximum temperature obtainable at fixed laser intensity. It is quite clear that a lower agglomerate concentration plays the role of a reduced amount of energy absorbed and therefore a consequent lower temperature. This point is verified for several fg-Si layer thicknesses. We argue that inelastic scattering of incoming radiation on the walls of octahedral micrograins determines a phonon production responsible of local temperature increase.

In previous papers we investigated the phonon behavior as a function of temperature for Raman spectra at similar laser rate. Here, as clearly visible in PL spectra, the Raman peak is progressively reduced when the PL grows, indicating the huge competition of phonon absorption for electron indirect excitations with respect to Raman scattering^{22,23}. In other words, at high temperature indirect transitions deplete Raman absorption, populating excited states responsible of PL decay. This cannot happen for too weak laser rate, i.e., at low temperature, because a threshold for phonon accumulation should be reached.

The localization of hot carriers, in a range of the order of 1 micrometer, is also demonstrated by the possible use of a polymeric (low melting point) substrate. This proves the excellent thermal insulating properties of fg-Si. Furthermore, thermalization of hot excited carriers with phonon production is unlike, since this contribution increasing the local temperature should be present at any deposition thickness, in contrast with the experiment. Actually, PL emission was detected in the wide visible range up to 925 nm. Beyond this value, i.e., in the IR range around the Si gap (1.12 eV) the PL emission was negligible. Therefore, before decay, the hot carriers do not lose energy for thermalization. The broad PL spectrum covers the wide range from the red wavelength up to the visible border. A further investigation of the lifetime as a function of the frequency, could add information on the relative percentages between radiative and non-radiative processes distinguishing direct and indirect processes,

and allowing the determination of specific quantum yield of emitted PL³².

The proposed explanation should be discussed in the light of alternative possible causes of the observed effect. We exclude the presence of crystallographic defects, as confirmed by high resolution TEM analysis (not shown) in several, individual octahedra. Also H-defects could in principle contribute a donor impurity level, but the presence of high amount of hydrogen is unlike because the formation process of nanoparticles occurs by the expulsion of hydrogen²⁴. Moreover Hydrogen degases quickly at relatively low temperature (400°C), and therefore cannot influence the PL emission at least at the highest temperatures³³. In contrast, a substoichiometric oxide layer formed when the fg-Si is exposed to air after deposition can enhance the effect because of two reasons: the first is related to a possible action as antireflection coating of the incoming radiation, the second could be due to a phonon trapping by the surface oxide³².

In summary we have demonstrated that a large PL stimulation is produced with a PL increment with respect to the reference sample of the order of a factor 5000 with an optical gain value as high as 0.14 cm/W. The innovative contribution of hot phonons prevents the thermalization of hot carriers, determining giant PL emission. A possible extension of this method to a reduced size ensemble, with an increased gap, size dependent, could produce PL amplification at higher frequency. The synthesis method based on chemical vapour deposition reactor is fully compatible with all Si based technologies and therefore we expect this innovative material could find applications in optoelectronics and in the photovoltaic field, and be further enhanced by proper impurity doping. The entire deposition process and PL emission is compatible with flexible and low cost substrate.

Methods

Samples are prepared in vacuum (5×10^{-7} Torr) in an inductively coupled plasma chemical vapour deposition reactor exploiting the capability of this "non-thermal" plasma to enhance Si crystalline nanoparticles formation, rather than SiH_4 decomposition into amorphous Si deposition²⁴. This reactor has a vertical geometry, the plasma is highly ionised ($2 \div 6 \times 10^{11}/\text{cm}^3$) and the substrate is maintained at low temperature (50°C). Process pressure is instead in the 5–30 mTorr range. Deposition is performed on a 6 inches area. Depending on the plasma parameters used (pressure, time, RF power) Si nanoparticles have a variety of equilibrium shapes²⁷. The density of the fg-Si layer is controlled by performing the process for a specific time and eventually repeating the process as many times as needed to pile up nanoparticles up to the desired thickness.

The sample are analyzed by transmission electron microscopy (TEM) microscopy using a JEOL JEM 2010 microscope with a LaB6 thermoionic source, operating at an acceleration voltage of 200 kV and equipped with a Gatan multiscan digital camera. After proper sample thinning, all the analyses are carried out in bright field condition.

X-ray diffraction analyses are performed by using a high angular resolution D8Discover Bruker AXS diffractometer equipped with a $\text{K}\alpha\text{Cu}$ source, a Goebel mirror and long sollar slits.

The samples are investigated by micro Raman spectroscopy for detecting the transversal optical (TO) vibrational peak situated for bulk Si at 521 cm^{-1} , at room temperature (300 K). Raman and PL spectra are collected in backscattering geometry with a HORIBA Jobin-Yvon system, equipped with Olympus BX41 microscope. He-Ne laser radiation at a wavelength of 632.8 nm is focused to a spot size of the order of $1 \mu\text{m}$ by a $100\times$ objective. The laser power on the sample is 6 mW, and a 550 mm focal length spectrometer with 1800 lines/mm grating is used for collecting Raman spectra. PL measurements are performed with the same apparatus used for the Raman spectroscopy using a 600 lines/mm grating and extending the observation range from 640 nm up to 1150 nm.

- Belyakov, V., Burdov, V., Lockwood, R. & Meldrum, A. Silicon Nanocrystals: Fundamental Theory and Implications for Stimulated Emission. *Advances in Optical Technologies* **2008**, 1–32 (2008).
- Sirleto, L., Ferrara, M. A., Nikitin, T., Novikov, S. & Khriachtchev, L. Giant Raman gain in silicon nanocrystals. *Nature communications* **3**, 1220 (2012).
- Ledoux, G. *et al.* Photoluminescence properties of silicon nanocrystals as a function of their size. *Physical Review B* **62**, 15942–15951 (2000).
- Pavesi, L. & Turan, R. *Silicon Nanocrystals*. (Wiley-VCH Verlag GmbH & Co. KGaA, Weinheim: 2010).
- Luque, A. & Hegedus, S. *Handbook of Photovoltaic Science and Engineering Handbook of Photovoltaic Science and Engineering*. (John Wiley & Sons, Ltd: 2011).
- Liang, D. & Bowers, J. E. Recent progress in lasers on silicon. *Nature Photonics* **4**, 511–517 (2010).



7. Iacona, F., Bongiorno, C., Spinella, C., Boninelli, S. & Priolo, F. Formation and evolution of luminescent Si nanoclusters produced by thermal annealing of SiO₂ films. *Journal of Applied Physics* **95**, 3723 (2004).
8. Timmerman, D., Valenta, J., Dohnalová, K., de Boer, W. D. A. M. & Gregorkiewicz, T. Step-like enhancement of luminescence quantum yield of silicon nanocrystals. *Nature nanotechnology* **6**, 710–3 (2011).
9. Wen, X., Dao, Van L. & Hannaford, P. Temperature dependence of photoluminescence in silicon quantum dots. *Journal of Physics D: Applied Physics* **40**, 3573–3578 (2007).
10. Li, J. F. *et al.* Shell-isolated nanoparticle-enhanced Raman spectroscopy. *Nature* **464**, 392–5 (2010).
11. Nie, S. & Emory, S. Probing Single Molecules and Single Nanoparticles by Surface-Enhanced Raman Scattering. *Science* **275**, 1102–6 (1997).
12. Claps, R., Dimitropoulos, D., Raghunathan, V., Han, Y. & Jalali, B. Observation of stimulated Raman amplification in silicon waveguides. *Optics express* **11**, 1731–9 (2003).
13. Boyraz, O. & Jalali, B. Demonstration of a silicon Raman laser. *Optics express* **12**, 5269–73 (2004).
14. Rong, H. *et al.* An all-silicon Raman laser. *Nature* **433**, 292–4 (2005).
15. Schmidt, P., Berndt, R. & Vexler, M. Ultraviolet Light Emission from Si in a Scanning Tunneling Microscope. *Physical Review Letters* **99**, 246103 (2007).
16. de Boer, W. D. A. M. *et al.* Red spectral shift and enhanced quantum efficiency in phonon-free photoluminescence from silicon nanocrystals. *Nature nanotechnology* **5**, 878–84 (2010).
17. Fujii, M., Yamaguchi, Y., Takase, Y., Ninomiya, K. & Hayashi, S. Control of photoluminescence properties of Si nanocrystals by simultaneously doping n- and p-type impurities. *Applied Physics Letters* **85**, 1158 (2004).
18. Bude, J., Sano, N. & Yoshii, A. Hot-carrier luminescence in Si. *Physical Review B* **45** (1992).
19. Trinh, M. *et al.* Direct generation of multiple excitons in adjacent silicon nanocrystals revealed by induced absorption. *Nature Photonics* **6**, 316 (2012).
20. König, D. *et al.* Hot carrier solar cells: Principles, materials and design. *Physica E: Low-dimensional Systems and Nanostructures* **42**, 2862–2866 (2010).
21. Govoni, M., Marri, I. & Ossicini, S. Carrier multiplication between interacting nanocrystals for fostering silicon-based photovoltaics. *Nature Photonics* **6** (2012).
22. Faraci, G., Gibilisco, S. & Pennisi, A. R. Superheating of silicon nanocrystals observed by Raman spectroscopy. *Physics Letters A* **373**, 3779–3782 (2009).
23. Faraci, G., Gibilisco, S. & Pennisi, A. R. Quantum confinement and thermal effects on the Raman spectra of Si nanocrystals. *Physical Review B* **80**, 193410 (2009).
24. Kortshagen, U. Nonthermal plasma synthesis of semiconductor nanocrystals. *Journal of Physics D: Applied Physics* **42**, 113001 (2009).
25. Martin, P. M. *Handbook of deposition technologies for film and coatings*. (Elsevier: 2010).
26. Bapat, A., Gatti, M., Ding, Y.-P., Campbell, S. A. & Kortshagen, U. A plasma process for the synthesis of cubic-shaped silicon nanocrystals for nanoelectronic devices. *Journal of Physics D: Applied Physics* **40**, 2247–2257 (2007).
27. Barnard, A. S. & Zapol, P. A model for the phase stability of arbitrary nanoparticles as a function of size and shape. *Journal of Chemical Physics* **121**, 4276–83 (2004).
28. Stekolnikov, A. A. & Bechstedt, F. Shape of free and constrained group-IV crystallites: Influence of surface energies. *Physical Review B* **72**, 125326 (2005).
29. Yu, P. Y. & Cardona, M. *Fundamentals of semiconductors*. (Springer: 2010).
30. Gibilisco, S., Faraci, G., Pennisi, A. R. & Irrera, A. Laser induced heating of Si nanocrystals. *Journal of Non-Crystalline Solids* **356**, 1948–1950 (2010).
31. Faraci, G., Gibilisco, S., Russo, P., Pennisi, A. & La Rosa, S. Modified Raman confinement model for Si nanocrystals. *Physical Review B* **73**, 033307 (2006).
32. Faraci, G. *et al.* Catalytic role of adsorbates in the photoluminescence emission of Si nanocrystals. *Physical Review B* **78**, 245425 (2008).
33. Beyer, W. Determination of the hydrogen diffusion coefficient in hydrogenated amorphous silicon from hydrogen effusion experiments. *Journal of Applied Physics* **53**, 8745 (1982).

Acknowledgements

We are grateful to Antonino La Magna and Vittorio Privitera (CNR-IMM) for useful discussions and to Corrado Bongiorno (CNR-IMM) for his expertise in transmission electron microscopy analyses. This work has been done with the support of Italian project PON02_00355_3391233-Tecnologie per l'ENERGIA e l'Efficienza energeETICa-ENERGETIC.

Author contributions

G.F. conceived the study; G.F., A.R.P. and G.M. equally contributed to this research; G.F., A.R.P., A.A. and G.M. discussed the results at all stages. G.F. wrote the paper with extensive contributions from A.R.P., A.A. and G.M. G.M. prepared the samples, G.F. and A.R.P. carried out Raman and PL measurements, A.A. carried out the x-ray diffraction analyses and R.R. carried out electron microscopy analyses.

Additional information

Competing financial interests: The authors declare no competing financial interests.

How to cite this article: Faraci, G., Pennisi, A.R., Alberti, A., Ruggeri, R. & Mannino, G. Giant photoluminescence emission in crystalline faceted Si grains. *Sci. Rep.* **3**, 2674; DOI:10.1038/srep02674 (2013).



This work is licensed under a Creative Commons Attribution-NonCommercial-NoDerivs 3.0 Unported license. To view a copy of this license, visit <http://creativecommons.org/licenses/by-nc-nd/3.0>